Earth and Space Science

RESEARCH ARTICLE
10.1029/2019EA000910

Validation of Surface Temperature Derived From MERRA-2 Reanalysis Against IMD Gridded Data Set Over India

Priyanshu Gupta[1], Sunita Verma[1,2], R. Bhatla[3,2], Amit Singh Chandel[4], Janhavi Singh[1], and Swagata Payra[5]

[1]Institute of Environment and Sustainable Development, Banaras Hindu University, Varanasi, India, [2]DST-Mahamana Centre of Excellence in Climate Change Research, Banaras Hindu University, Varanasi, India, [3]Department of Geophysics, Banaras Hindu University, Varanasi, India, [4]Center of Environmental Sciences, University of Allahabad, Prayagraj, India, [5]Department of Physics, Birla Institute of Technology Mesra, Extension Centre Jaipur, India

Key Points:
- Validation of temperature data set (1981–2015) of MERRA-2 against IMD observation over India has been conducted
- MERRA-2 maximum temperature shows overestimation (~4%) over India except Western Himalaya with an underestimation of −82.5%
- The results may help in using MERRA-2 temperature for future study of extreme events after calibration with estimated errors over India

Correspondence to:
S. Payra,
spayra@gmail.com

Citation:
Gupta, P., Verma, S., Bhatla, R., Chandel, A. S., Singh, J., & Payra, S. (2020). Validation of surface temperature derived from MERRA-2 Reanalysis against IMD gridded data set over India. *Earth and Space Science*, *7*, e2019EA000910. https://doi.org/10.1029/2019EA000910

Received 25 SEP 2019
Accepted 1 DEC 2019
Accepted article online 12 DEC 2019

Abstract The first detailed validation of maximum temperature of Modern-Era Retrospective analysis for Research and Application Version 2 ($T_{MERRA\text{-}2}$) against Indian Meteorological Department (T_{IMD}) has been carried out for 35 years (1981–2015) over India. For this purpose, India has been divided into seven different zones, i.e Western Himalaya (WH), Northwest, North Central, Northeast (NE), West Peninsula India, East Peninsula India, and South Peninsula India. The descriptive statistics and correlation between $T_{MERRA\text{-}2}$ and T_{IMD} have been determined for monthly, seasonal, and annual basis. A significant correlation (>0.9) has been found for monthly $T_{MERRA\text{-}2}$ and T_{IMD} with a root-mean-square error value closer to 1 except for WH where a high root-mean-square error value of 18.2 is obtained. Seasonal analysis also indicates a significant correlation for all the zones except for WH and NE with a correlation value of <0.3 during monsoon season; this may be due to sparse network, cold climate, and heterogeneity due to topography. Percent bias indicates that $T_{MERRA\text{-}2}$ generally overestimates the T_{IMD} monthly observations for all the zones, that is, Northwest, North Central, NE, West Peninsula India, East Peninsula India, and South Peninsula India by 4.1%, 2.4%, 1.6%, 0.5%, 0.2%, and 0.8%, respectively, except WH where an underestimation (−82.5%) is determined. Thus, after calibration, MERRA-2 Reanalysis maximum temperature may be used for further study of extreme weather events.

1. Introduction

Preindustrial time had less emission of greenhouse gases (GHG), mainly CO_2, into the atmosphere resulting in minor variation of temperature. Since the industrialization, there has been a noticeable increase in the emission of GHGs in the atmosphere, raising the surface air temperature of the atmosphere. Therefore, monitoring and analysis of surface air temperature on regional as well as global scale has gained special importance. Houghton et al. (2001) reported that the surface air temperature on the global and regional scales has increased significantly in the former century and distinct warming of climate has taken place in the past four decades. Global mean temperature has increased by about 0.4 °C/100 years over India during 1901–1982 (Hingane et al., 1985). Kothawale and Rupa Kumar (2005) studied that the mean maximum and minimum temperature over India has increased by 0.2 °C/100 years during 1971–2003. Hu et al. (2010) concluded that continuous increase in the concentration of GHG and changes in atmospheric circulation and climate forcing may causes the average increase of regional warm nights for all studied reanalysis products. The Intergovernmental Panel on Climate Change (IPCC) recorded the continuous increase of global mean surface air temperature by 0.6 °C in its third assessment report (IPCC, 2001) , by 0.74 ± 0.18 °C during the last century (1906–2005) in the fourth assessment report (IPCC, 2007), and by 1.5 °C at the end of the 21st century with respect to 1850–1900 in the fifth assessment report (IPCC, 2014).

The long-term trend and variation of global surface air temperature has been reported in several scientific studies. Surface temperature (ST) variation has been studied by Jones et al. (1982), Hansen et al. (1981), which helped to understand the heat island analysis and also contribute in the prediction system of regional level climatology as well as the trend analysis of the temperature variation at annual and seasonal scales. All these studies have pointed to the warming of the Northern Hemisphere. Global land and ocean

measurements of ST obtained through radiometers on satellites and ground-based observatories have made a contribution to climate research.

Satellite products are important tools for climate prediction and future climate change. Lai et al. (2012) compared the Moderate Resolution Imaging Spectroradiometer (MODIS) land ST with ground-based observed air temperature in complex topography. Liu et al. (2017) analyzed the MODIS land ST (Ts) with meteorological observed and ERA-Interim Reanalysis product over South China and obtained the root-mean-square difference value of 9.5–19.4 K between the MODIS Ts and the in situ Ts for all land types. According to the authors, these uncertainties may arise due to different land classes, topography, soil moisture, and surface water. Also, satellites cannot accurately describe the temperature variation due to their coarse resolution and low temporal resolution. Ground-based measurements are very good, but they are too limited in spatial resolution. There is a need of collecting information by promoting the interdisciplinary and multisensor research by using a combination of satellite retrievals, numerical models, reanalysis products, and also ground-based in situ measurements. Models have good simulation ability for the global and regional scales in measurement of precipitation and temperature.

The systematic overestimation or underestimation of climatic variables by any climate model is known as bias and may rely on climatological and geographical factors and also on the choice of the climate model (Hagemann et al., 2011; Maity et al., 2019; Mao et al., 2015; Maraun et al., 2017). Fan and Van den Dool (2008)) in their study found the biases between reanalysis product against observed, that is, the Global Historical Climatology Network version 2 + Climate Anomaly Monitoring System, which vary according to season and with global domain. Various methods are used to calibrate the meteorological parameters. Bias correction is a statistical adjustment of the modeled or reanalysis products toward the reference products. It can be done by following various procedures. One of the ways is to develop a transfer function in order to match the cumulative distribution function (CDF) of observed and modeled/reanalysis data sets from large-scale variables (such as precipitation and temperature), such as equidistant CDF matching method and CDF transform method (Guo et al., 2018). CDF transform method is used in many scientific studies to do bias correction of temperature and precipitation of different regions of the world and has gained better results such as in Michelangeli et al. (2009), Lavaysse et al. (2012), Flaounas et al. (2013), and Vigaud et al. (2013). Li et al. (2010) introduced the equidistant CDF matching method on the basis of equidistant quantile mapping in doing bias correction of temperature and precipitation in northern Europe. Hoffmann et al. (2016) in their study for climatological bias as well as interannual variance correction introduced bias and variance correction method, which applies a simple algorithm especially in the tropics region. A vast number of variables such as state and availability of water, solar angle, radiative properties of atmosphere, albedo, type and formation of clouds, and wind movement are associated with the surface air temperature in the lower atmosphere (Willmott, 1987).

Modern-Era Retrospective analysis for Research and Application Version 2 (MERRA-2) represents the modified version of MERRA and was recently released by NASA's Global modeling and Assimilation office (Gelaro et al., 2017). MERRA-2 having an ongoing near-real-time climate analysis gained a significant improvement in compared to its predecessor, that is, MERRA. It included an update to the Goddard Earth Observing System model and analysis scheme which helps in climate analysis. It also considered the future Integrated Earth System analysis that includes aerosol data assimilation and improved representation of the cryosphere and stratosphere including ozone. This ongoing development addresses several other improvements in MERRA-2 version, that is, assimilation of satellite observations, reduction in certain biases, and water cycle imbalances.

The MERRA-2 data sets have been analyzed by several authors previously (Bosilovich et al., 2017; McCarty et al., 2016). Hearty et al. (2018) compared the AIRS, MERRA, and MERRA-2 near-surface air and skin temperature with National Oceanic and Atmospheric Administration temperature at the Summit, Greenland. The authors found the improvements of MERRA-2 data over MERRA with a little sensitivity to temperature inversions.

This is the first time that an extensive validation of MERRA-2 maximum temperature ($T_{\text{MERRA-2}}$) against the Indian Meteorological Department (IMD) observed maximum temperature (T_{IMD}) over India has been carried out in detail. The main objective of the study is to compare and analyze the long-term (35 years)

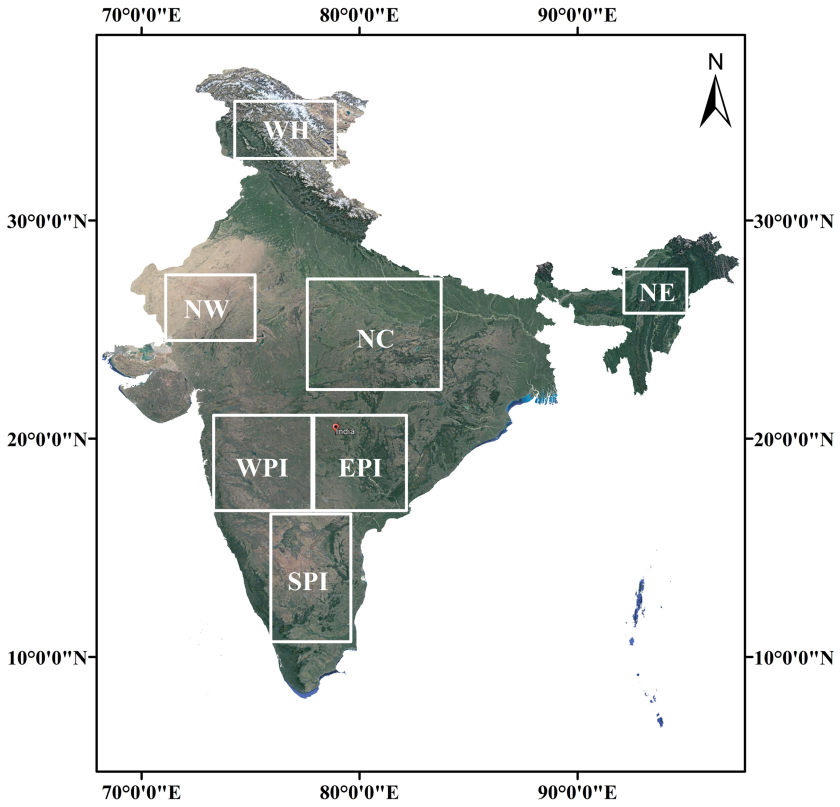

Figure 1. Map of India showing the seven selected regions on the basis of temperature homogeneity.

variations of average maximum temperature and to validate MERRA-2 reanalysis product with ground-based IMD data sets over India by considering seven different zones.

The paper comprises five sections: Sections 1, 2, and 3 deal with detailed description of data extraction, methodology, and site description, whereas section 4 describes the results using different statistical methods. In section 4.1 different descriptive statistics to quantify the uncertainties of MERRA-2 with reference to ground-based observed data set as a standard are described. Section 4.2 of the study deals with the variation of observed as well as reanalyzed products for 35 years. Seasonal variations of maximum temperature and their respective biasness are depicted by spatial patterns in section 4.3, whereas intercomparison of average maximum temperature of MERRA-2 and IMD data for different months are shown in section 4.4. Further, a Taylor diagram and correlation matrix are discussed in sections 4.5 and 4.6, respectively. Finally, section 5 concludes with main points drawn from the study.

2. Data Analysis and Methodology

2.1. IMD Observations

In this study, we have used the daily maximum temperature data sets at 1° × 1° grid resolutions (Rajeevan et al., 2008) derived from IMD at 2 m height for the period 1981–2015. The observation has been then differentiated as seven different zones of India, that is, Western Himalaya (WH), Northwest (NW), North Central (NC), Northeast (NE), West Peninsula India (WPI), East Peninsula India (EPI), and South Peninsula India (SPI) as shown in Figure 1 for a detailed analysis and validation.

2.2. MERRA-2 Reanalysis Data

Surface air temperature data sets at 2 m height for the period 1981–2015 are obtained from MERRA-2 which provides data at 0.5° × 0.625°grid resolution (Gelaro et al., 2017); it is further regridded to 1° × 1° resolution, the same as for observed IMD data sets.

Table 1
Seven Zones of India With Their Respective Coordinates

Regions	Coordinates	
	Latitude	Longitude
Western Himalaya (WH)	32.84–35.46°N	74.27–78.88°E
Northwest (NW)	24.5–27.5°N	70.8–75.2°E
North Central (NC)	22.25–27.32°N	77.69–83.74°E
Northeast (NE)	25.75–27.77°N	92.12–94.9°E
West Peninsula India (WPI)	16.70–21.07°N	73.20–77.81°E
East Peninsula India (EPI)	16.70–21.07°N	77.90–82.24°E
South Peninsula India (SPI)	10.69–16.55°N	75.93–79.74°E

MERRA-2 with a horizontal resolution of 0.5° latitude by 0.625° longitude and 72 vertical layers begins in the year 1980. Because of the advancement made in assimilation of modern hyper spectral radiance, GPS-radio occultation and microwave observation data sets of MERRA-2 enable us to replace the original MERRA data set. Additional advancement in the Goddard Earth Observing System atmospheric model (Molod et al., 2015) and the Grid point Statistical Interpolation analysis scheme (Kleist et al., 2009) are considered as the key components of the MERRA-2 model. During late 2004 it also began to use NASA's ozone profile observations.

In addition to meteorological assimilation, MERRA-2 is the first long-term global reanalysis product which assimilates space-based observations of aerosols in climate system and represents their interactions with physical processes.

2.3. Methodology

The present paper discusses the validation of MERRA-2 temperature product ($T_{\text{MERRA-2}}$) against IMD temperature (T_{IMD}) observations for the period 1981–2015. The maximum temperature data sets are extracted for MERRA-2 and IMD for seven different zones of India. According to IMD seasons have been divided as winter season (January to February), summer season (March to May), monsoon season (June to September), and postmonsoon season (October to November) for the analysis over India. The details of descriptive statistics used can be found in Appendix A.

3. Study Area

India is in the Northern Hemisphere lying at 8°4′–37°6′N and 68°7′–97°25′E. India accounts about the 2.4%(about 3.28 million Km^2) of the world's total geographic area and ranked at seventh position among the world countries. India has a diverse and complex type of geographical area. Thus, the effects of climate change over India are also highly variable. In order to better examine the changes in temperature, India has been divided into seven different zones on the basis of temperature as shown in Figure 1. These seven zones (Figure 1) are the WH, NW, NC, NE, WPI, SPI, and EPI. The WH zone covers Jammu and Kashmir and a part of Himachal Pradesh having low temperature throughout the year and high-altitude mountains usually covered with snow. The NW zone covers the state of Rajasthan. This region has mostly semiarid and dry climate. The NC part covers the states of Uttar Pradesh, Madhya Pradesh, some part of Chhattisgarh, and Jharkhand. The NE zone covers Assam and some part of Arunachal Pradesh and Nagaland. The southern part of the country known as Interior Peninsula has been divided into three parts: WPI covers the states of Maharashtra, Goa, and part of Karnataka; SPI includes the states of Tamil Nadu, Kerala, part of Andhra Pradesh, and Karnataka; and EPI covers the states of Telangana, Chhattisgarh, Orissa, and Andhra Pradesh. The selection of site from each region is done by covering the maximum area of that region.

4. Results and Discussions

4.1. Statistical Analysis

Different statistical methods (listed in Table 2) are applied for monthly maximum temperature MERRA-2 data sets over all seven zones, that is, WH, NW, NC, NE, WPI, EPI, and SPI.

Mean absolute error (MAE) is the simplest matrix used to quantify the average magnitude of the errors in a set of predictions without considering sign. It is observed from Table 1 that the root-mean-square error (RMSE) is always greater than or equal to the MAE. Generally, a high value of MAE and RMSE reflects a bad predictive model or reanalysis product. In this study we find low values of MAE and RMSE, that is, 1.02 and 1.25 for SPI, whereas high values of MAE and RMSE (17.9 and 18.2) are reported over WH, which reveals a large difference between reanalysis and observational values. Furthermore, Willmott and Matsuura (2006)) in their study have reported that RMSE is dependent on geographic area and time period; it often increases when these variables increase because greater numbers of outliers are more likely in larger sampling domains. The percentage bias, index of agreement, correlation coefficient, and coefficient of determination matrices are also evaluated. Over NW (4.1%), NC (2.4%), NE (1.6%), WPI (0.5%), EPI (0.2%), and SPI

Table 2
Statistical Measures of MERRA-2 Against IMD Observation

Statistical terms	Mathematical expression	Range	WH	NW	NC	NE	WPI	EPI	SPI
Mean absolute error (MAE)	$\frac{1}{n}\sum\lvert M-O\rvert$	0 to ∞	17.9	1.4	1.54	1.4	1.05	1.55	1.02
Root-mean-square error (RMSE)	$\sqrt{\frac{\sum_{1}^{n}(M-O)^2}{n}}$	0 to ∞	18.2	1.6	1.75	1.8	1.27	1.76	1.25
Percent bias (PBIAS)	$100\times\left[\sum^{(M-O)}/_{\sum(O)}\right]$	0 to ±∞	−82.5	4.1	2.4	1.6	0.5	0.2	0.8
Index of agreement (d)	$d=1-\frac{\sum_{i=1}^{n}(O_i-M_i)^2}{\sum_{i=1}^{n}\left(\lvert M_i-\overline{O}\rvert+\lvert O_i-\overline{O}\rvert\right)^2}$	$0\le d\le 1$	0.51	0.98	0.97	0.93	0.97	0.96	0.96
Correlation coefficient (r)	$r=\frac{\sum_{i=1}^{n}(O_i-\overline{O})(M_i-\overline{M})}{\sqrt{\sum_{i=1}^{n}(O_i-\overline{O})^2}\sqrt{\sum_{i=1}^{n}(M_i-\overline{M})^2}}$	$-1\le r\le +1$	0.96	0.99	0.96	0.9	0.96	0.95	0.94

(0.8%) positive values of percent bias (PBIAS) are obtained which indicates overestimation of reanalysis data, whereas in the case of WH (−82.5%) the reanalysis product seems to be underestimated. A better degree of agreement is found between reanalysis and observed data for NW (0.98), NC (0.97), WPI (0.97), EPI (0.96), SPI (0.96), and NE (0.93) with poor agreement for WH (0.51). Correlation coefficient is observed to be 0.96, 0.99, 0.96, 0.90, 0.96, 0.95, and 0.94 for WH, NW, NC, NE, WPI, EPI, and SPI, respectively.

Overall, statistics reveal good correlation. Table 2 shows a good correlation of 0.99 for NW zone. The best RMSE value is close to 0, indicating a perfect fit of the data. In this study the best RMSE is observed for SPI (1.25), whereas the minimum bias (0.2) is captured for EPI. A closer look reveals that NW has the best agreement (0.98), while WH has least (0.51).

4.2. Long-Term Annual Variations

Figure 2 displays the long-term (35 years) variation in annual maximum temperature of T_{IMD} and $T_{\mathrm{MERRA\text{-}2}}$ data sets. T_{IMD} shows a mean and standard deviation of 21.72 ± 0.63(WH), 28.87 ± 0.59 (NE), 32.93 ± 0.58(NW), 32.03 ± 0.44(NC), 33.15 ± 0.36(EPI), 32.85 ± 0.33(WPI), and 32.14 ± 0.25(SPI). For T_{IMD} the maximum value of standard deviation is observed for WH followed by NE with minimum value for SPI zone. MERRA-2 reveals a mean and standard deviation value of 3.89 ± 0.90, 34.28 ± 0.70, 32.81 ± 0.62, 29.38 ± 0.48, 32.99 ± 0.47, 33.21 ± 0.46, and 32.41 ± 0.44 for WH, NW, NC, NE, WPI, EPI, and SPI, respectively.

4.3. Spatial Distribution: MERRA-2 Versus IMD

This section describes the spatial distribution of long-term (35 years) average maximum temperature data sets for four different seasons. From Figure 3a it is observed that during winter, due to high elevation, WH belt experiences relatively cold temperature, which ranges from −10 to 5 °C as shown in MERRA-2 data (upper panel), while it ranges from 10–15 °C for IMD data (lower panel). The NE belt experiences average maximum temperature that ranges from 5–25 °C as shown in Figure 3a. There is progressive shift of higher (35 °C) to lower (−10 °C) temperature from the southern to northern part of India as during winter the intensity of the sun is much more pronounced over southern India. Further, from the bias estimation of MERRA-2 against IMD ($T_{\mathrm{MERRA\text{-}2}}$-$T_{\mathrm{IMD}}$) (right panel) it is revealed that MERRA-2 is overestimated over most of the zones by 1 to 4 °C except over WH and NE where an underestimation within a range of −6 to +1 °C is observed.

India experiences summer season from March to May. Figure 3b shows that during summer season WH experiences average maximum temperature between 0 and 15 °C (MERRA-2 data) and between 20 and 25 °C (IMD data), which indicates underestimation of MERRA-2 compared to IMD product in WH region. The central and southern parts of India show average maximum temperature range between 35 and 40 °C. MERRA-2 reanalysis data in the central and southern parts of India show overestimation in the range of −1

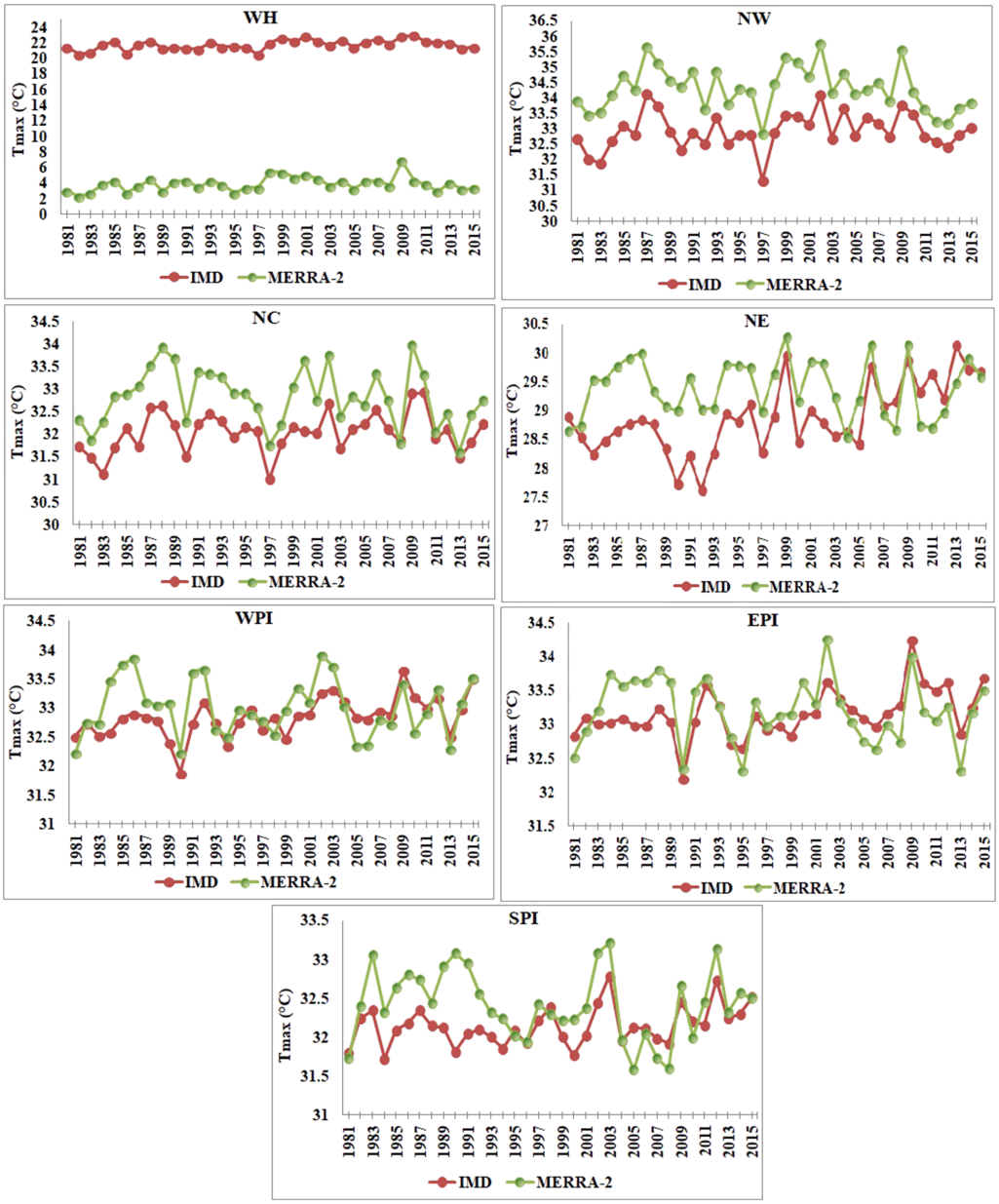

Figure 2. Variation of annual maximum temperature during 1981–2015.

to 3 °C, whereas the lower northern plain and regions around the Bay of Bengal depict bias in the range of 2 to 5 °C.

The month of June marks the onset of the monsoon in most of the region; it remains up to the month of September. Figure 3c shows that during the monsoon, WH and NE experiences milder weather than elsewhere in India with average maximum temperature range of 5–30 °C for MERRA-2 (upper panel) and 25–30 °C for IMD (lower panel). Toward NW, part of India's monsoon season has average maximum temperature between 35 and 40 °C; it experiences semiarid climate with minimal rainfall in Thar Desert region. NC and the southern part of India show temperature in the range of 30–35 °C, whereas western coastal region indicates temperature in the range of 25–30 °C; it may be due to the sea breeze effect. During monsoon season MERRA-2 and IMD shows uncertainties in the range of −6°C to −3°C(WH) and −6 °C to 1 °C (NE), which indicates underestimation of MERRA-2 maximum temperature datasets whereas in remaining places it undergoes overestimation.

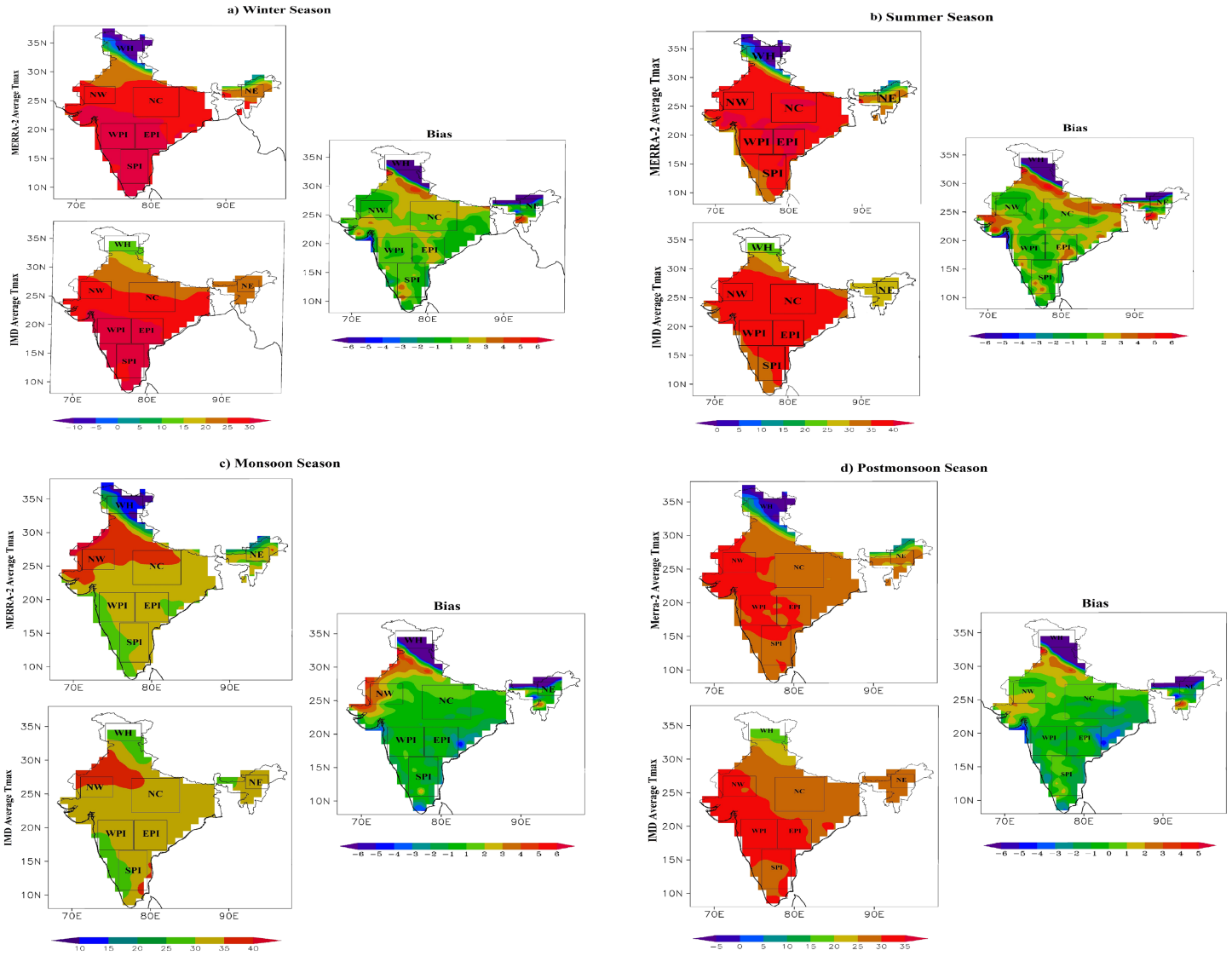

Figure 3. Spatial plot presenting seasonal variation of maximum ST of MERRA-2 and IMD data sets and their respective biasness for (a) winter season (b) premonsoon season, (c) monsoon season, and (d) postmonsoon season.

Postmonsoon season is characterized by retreating monsoon, that is, bringing of northeast monsoon with cool, dry, and dense air masses over maximum parts of India. Figure 3d presents 35 years average maximum temperature of MERRA-2 reanalysis and IMD data sets. It is observed that during postmonsoon season the average maximum temperature varies from −5 to 35 °C over different parts of India. Over WH MERRA-2 recorded maximum temperature in the range of −5 to 10 °C. Northern Plain as well southern peninsula depicts temperature range of 25 to 30 °C for both MERRA-2 and IMD data sets. In NW region maximum temperature reaches up to 30 to 35 °C. Furthermore, uncertainty studies show underestimation of MERRA-2 data in coastal, WH, NE, and some places of central and southern India. Bias within a range of 0 to 3, −2 to 2, and −3 to 1 °C is observed toward the northern, central, and southern regions of India.

4.4. Comparative Analysis: MERRA-2 Versus IMD

Figure 4 shows a box-whisker plot of the seven selected zones (WH, NW, NC, NE, WPI, SPI, and EPI). Figure 4 illustrates the comparative analysis of IMD as well as the MERRA-2 data. The boxes in each graph show the range of values and the whiskers represent the standard deviation. The hollow circles placed up

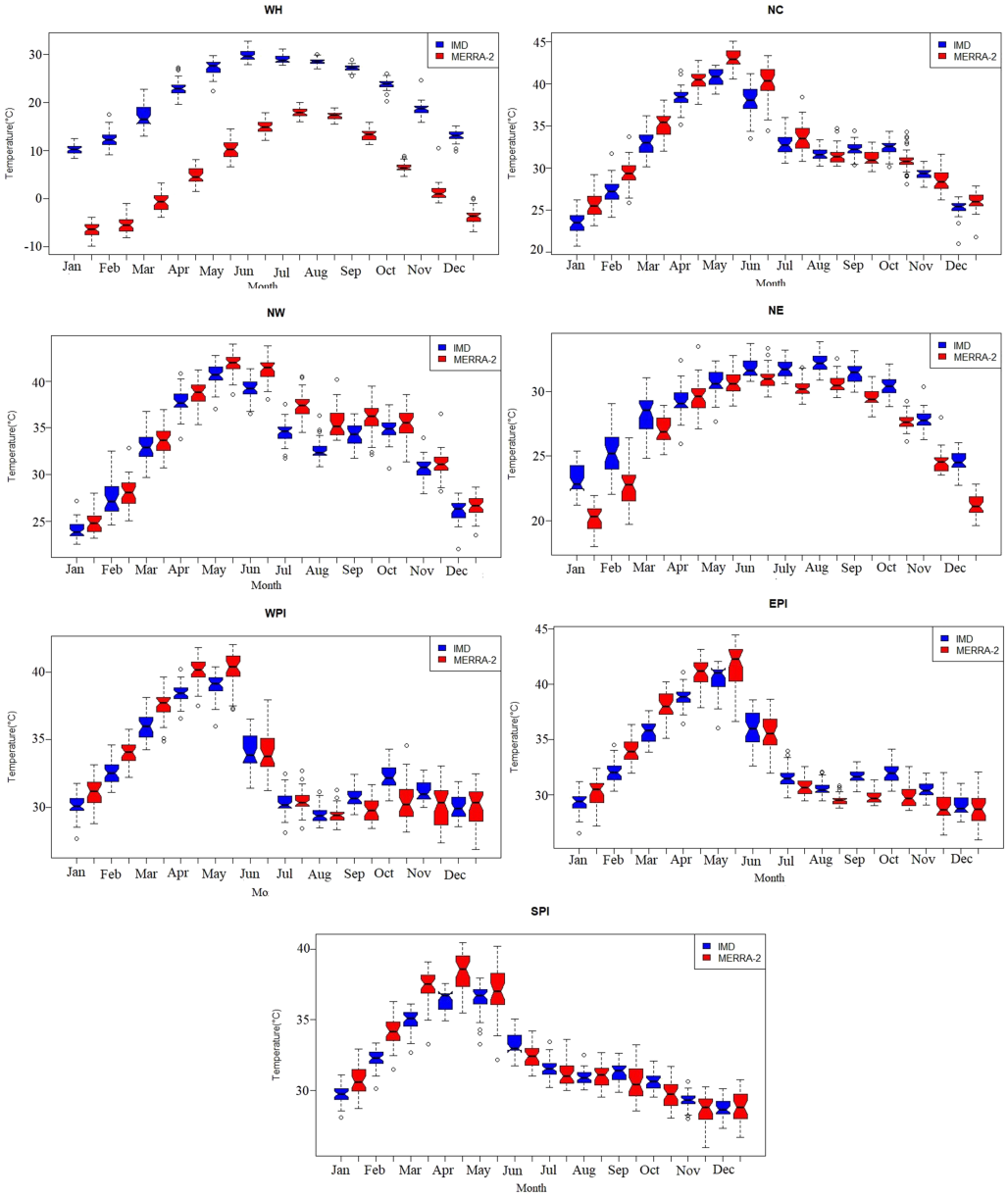

Figure 4. Box plots showing comparative analysis of MERRA-2 to observe for mean monthly temperature during 1986–2015. (a) WH, (b) NC, (c) NW, (d) NE, (e) WPI, (f) EPI, and (g) SPI.

and down sides of the whiskers are the outliers. The outliers represent the extreme high and low. The box plots correspond to 75th percentile (top line), median (middle line), and 25th percentile (lower line) of temperature values measured by the IMD and MERRA-2. The steepness in the box toward the median value is called notch, and it represents the 95% confidence interval of the median. Figures 4a (WH) and 4d. (NE) show similar pattern due to being close to the Himalayan region. WH and NE show a distinct increase in temperature range from January to July and then further decrease from July to December. However, in WH zone, IMD and MERRA-2 values show large variation whereas, in case of NE, IMD and MERRA-2 values are not same but very close to each other. The difference in the temperature values in case of WH may be due to error in measurement. On the other hand the NC and NW, that is, Figures 4b and 4c, respectively, have similar pattern of temperature trend. Sharp increase in the temperature values from January to June can be seen and further decrease to August, stable to October and further decrease

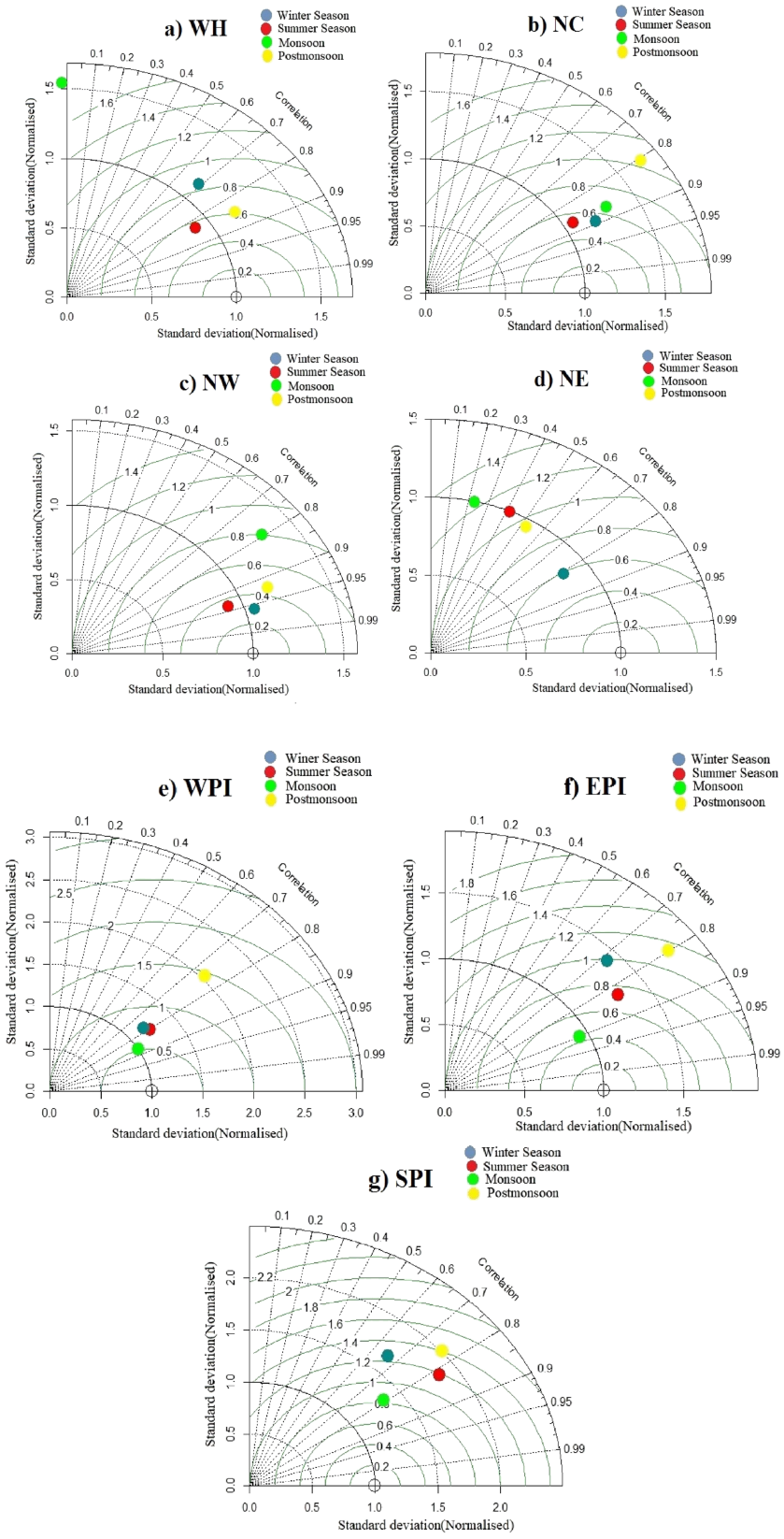

Figure 5. Taylor plot presents statistical correlation for different seasons. (a) WH, (b) NC, (c) NW, (d) NE, (e) WPI, (f) EPI, and (g) SPI.

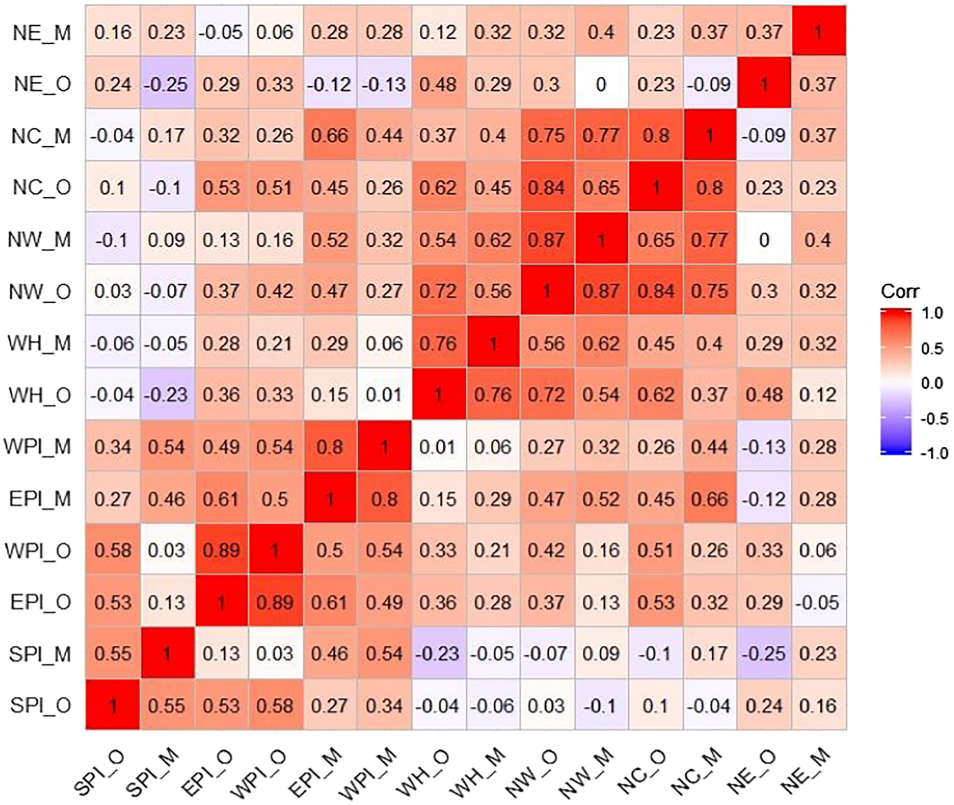

Figure 6. Correlation matrix plot showing correlation coefficient between seven zones of India

to December. The Peninsular regions (i.e., WPI, SPI, and EPI) also show similar trends, with increase in temperature (30 to 43 °C) from January to May and then gradual decrease of approximately 29 to 27 °C in July. With the Sun being present in the summer solstice during the month of June, NC and NW have higher temperature values in comparison to WPI, SPI, and EPI. More energy is trapped by the water molecule due to hygroscopic growth resulting in increase in the temperature during monsoon season, that is, from July to September. Over WPI and EPI the maximum temperature is observed during May due to alignment of the Sun over this region, subsequently fall in temperature is observed from May to July. Sun being in the winter solstice during the month of December, the sites have the lowest temperature values as they are in the Northern Hemisphere.

4.5. Taylor Diagram for MERRA-2 and IMD Observations

A graphical representation of the Taylor diagram helps to quantify the statistical correlation, standard deviation, and center root-mean-square difference of two different sets of data. In this section we show correlation and standard deviation of MERRA-2 with IMD observed data set during winter, summer, premonsoon, and postmonsoon seasons. As shown in Figure 5a during winter, summer, and postmonsoon correlation of 0.69, 0.83, and 0.85 is observed over WH, while a lower correlation (<0.02) is found during monsoon seasons. Over NW region good correlations of 0.96, 0.94, 0.79, and 0.92 are observed for all the seasons. From Figure 5c statistical correlation of MERRA-2 with IMD observed reveal correlation of 0.9, 0.88, 0.89, and 0.8 during winter, summer, monsoon, and postmonsoon seasons, respectively. It is observed from Figure 5d that over NE a correlation of 0.80 is found during winter, while a low correlation (<0.55) is observed during all the seasons. During monsoon WPI, EPI, and SPI zones show a high correlation of 0.89, 0.9, and 0.8, respectively.

Overall, the Taylor plots show that MERRA-2 has good performance during all seasons over NW, NC, WPI, EPI, and SPI, while it does not perform well over hilly regions, that is, WH and NE especially during monsoon season. This could be due to heterogeneity in topography which is not reproduced well by reanalysis data during monsoon season.

4.6. Correlation Matrix for Different Zones of India

MERRA-2 (reanalysis data) is intercorrelated and intracorrelated with IMD (observed data) for the seven different zones of India (WH, NW, NE, NC, WPI, EPI, and SPI) as shown in Figures 5 and 6. A symmetrical square matrix shows the same variables in rows and columns; the diagonal line indicates the perfect correlation of each variable with itself. Correlation below the diagonal line is the mirror image of the above values. High correlation between IMD and MERRA-2 can be seen in case of northern India except NE which has the lowest correlation, that is, 0.37, whereas moderate correlation can be seen in the peninsular region of India which may be due to lesser distance from sea. NW zone shows the best correlation (i.e., 0.87), and NE shows the minimum correlation (0.37). The MERRA-2 reanalysis and IMD observed values are highly intracorrelated (NC_M and NW_M have 0.77, EPI_M and WPI_M have 0.8, WPI_O and EPI_O have 0.89, and NC_O and NW_O have 0.84 correlation value). The intracorrelation between the adjacent areas shows the authenticity of the instrument and the intercorrelation between the observed and reanalyzed values shows the accuracy of the instrument in Figure 6. The symbol M refers to MERRA-2 reanalysis data while the symbol O refers to the IMD observations in this section or elsewhere.

5. Conclusions

This paper provides the validation of maximum ST MERRA-2 ($T_{\text{MERRA-2}}$) against IMD (T_{IMD}) data sets. Various statistical analyses have been used to validate MERRA-2 data sets with respect to IMD observations for seven homogenous zones of India during 1981 to 2015. In case of monthly maximum temperature MERRA-2 data is found to be highly correlated (>0.9) over all chosen zones of India. However, MERRA-2 was found to be less correlated with IMD observations especially over WH and NE in seasonal analysis especially during the monsoon season. Percentage bias indicates overestimation of MERRA-2 by 4.1%, 2.4%, 1.6%, 0.5%, 0.2%, and 0.8% over NW, NC, NE, WPI, EPI, and SPI, respectively, except WH where underestimation by −82.5% is determined. The reason for such underestimation might be the data scarcity problem of hilly regions due to disperse network, cold climate, and topography heterogeneity.

Additionally, seasonal variation of average maximum temperature for MERRA-2 and IMD data shows good result for time period of 1981 to 2015. MERRA-2 underestimated the temperature within a range of −6 to −3 °C toward hilly region and overestimated the temperature over other parts of India. It has been seen that for all the zones MERRA-2 temperature seems to be high as compared to IMD except WH and NE. Further, the square matrix table depicts correlation between and among the seven different zones of India for both MERRA-2 and IMD data sets on annual basis. From the matrix plot it has been concluded that except NE, all the regions toward northern part of India show good intracorrelation (>0.76); however, a low correlation (<0.60) is observed over southern zones and vice versa.

Overall, MERRA-2 maximum temperature data matches well with IMD observed data sets with an uncertainty of ±6 °C. Large difference of uncertainties is however observed over hilly regions especially for WH, India.

Appendix A

Different statistical methods are used to validate and compare IMD and MERRA 2 maximum temperature data sets

1. *MAE*: MAE is an important statistic used to measure average error. To obtain total error it sums the magnitude of the errors and then dividing it by total error by total number of observations, that is, n. It is expressed as

$$\text{MAE} = \frac{1}{n}\sum_{1}^{n}|M-O|$$

2. *RMSE*: RMSE is the most widely used error reported in the field of climatology, regression analysis, and forecasting. It determines how the data sets are concentrated around the line of best fit, considered as one

of the best methods to diminish the effect of extreme outliers by taking the difference betwee the model and actual value. It ranges from 0 to ∞, and a value of 0 indicates a perfect fit of the data.

$$\mathrm{RMSE} = \frac{\sqrt{\sum_{1}^{n}(M-O)^2}}{n}$$

3. *PBIAS*: Percentage bias is used to determine whether the model value is smaller or larger than the observed ones. Positive values show overestimation of bias, whereas negative values indicate underestimation of model data.

$$\mathrm{PBIAS} = 100\times[\sum(M-O)/\sum(O)]$$

4. *Index of agreement* (*d*): Willmott (1984) defined the index of agreement as the ratio of the mean square error and the potential error (PE) multiplied by *N* (number of observations) and then subtracted from 1. It varies from 0 to 1; higher value 1 reveals high agreement of model with observed, whereas 0 indicates no agreement. The index of agreement is calculated as follows:

$$d = 1-\frac{\sum_{i=1}^{n}(O_i-M_i)^2}{\sum_{i=1}^{n}\left(|M_i-\overline{O}|+|O_i-\overline{O}|\right)^2}$$

Where O_i refers to observation data and M_i shows the prediction or model data.

5. Correlation coefficient (*r*): Coefficient of correlation is used to measure degree of linear relationship between two data series. It lies between −1 and +1; *r* value equal to +1 indicates perfect and positive correlation, whereas negative value of −1 shows negative and perfect correlation. If *r* is equal to 0 it means there is no correlation between the variables; they are said to be independent.

Pearson correlation coefficient is calculated as follows:

$$r = \frac{\sum_{i=1}^{n}\left(O_i-\overline{O}\right)\left(M_i-\overline{M}\right)}{\sqrt{\sum_{i=1}^{n}\left(O_i-\overline{O}\right)^2}\sqrt{\sum_{i=1}^{n}\left(M_i-\overline{M}\right)^2}}$$

where *n* is the total sets of model data or station-observed data; *O* and *M* are the observed data and model data, respectively; and $\overline{M}$ and $\bar{O}$ are the average values of model data and observed data, respectively.

Acknowledgments
The authors wish to thank the India Meteorological Department, (IMD) and Modern-Era Retrospective analysis for Research and application Version 2 (MERRA-2) (https://gmao.gsfc.nasa.gov/reanalysis/MERRA-2/data_access/) for providing the necessary facilities to collect temperature data. The first author would like to thank Manish Soni for initial help related to graphics. The corresponding author would like to express thanks for funding support under Ministry of Earth Science (MoES) Project (MoES/16/18/2017-RDEAS).

References

Bosilovich, M. G., Robertson, F. R., Takacs, L., Molod, A., & Mocko, D. (2017). Atmospheric water balance and variability in the MERRA-2 reanalysis. *Journal of Climate*, *30*(4), 1177–1196. https://doi.org/10.1175/JCLI-D-16-0338.1

Fan, Y., & Van den Dool, H. (2008). A global monthly land surface air temperature analysis for 1948–present. *Journal of Geophysical Research*, *113*, D01103. https://doi.org/10.1029/2007JD008470

Flaounas, E., Drobinski, P., Vrac, M., Bastin, S., Lebeaupin-Brossier, C., Stéfanon, M., & Calvet, J. C. (2013). Precipitation and temperature space–time variability and extremes in the Mediterranean region: Evaluation of dynamical and statistical downscaling methods. *Climate Dynamics*, *40*(11-12), 2687–2705. https://doi.org/10.1007/s00382-012-1558-y

Gelaro, R., McCarty, W., Suárez, M. J., Todling, R., Molod, A., Takacs, L., et al. (2017). The Modern-Era Retrospective analysis for Research and Applications, version 2 (MERRA-2). *Journal of Climate*, *30*(14), 5419–5454. https://doi.org/10.1175/JCLI-D-16-0758.1

Guo, L. Y., Gao, Q., Jiang, Z. H., & Li, L. (2018). Bias correction and projection of surface air temperature in LMDZ multiple simulation over central and eastern China. *Advances in Climate Change Research*, *9*(1), 81–92. https://doi.org/10.1016/j.accre.2018.02.003

Hagemann, S., Chen, C., Haerter, J. O., Heinke, J., Gerten, D., & Piani, C. (2011). Impact of a statistical bias correction on the projected hydrological changes obtained from three GCMs and two hydrology models. *Journal of Hydrometeorology*, *12*(4), 556–578. https://doi.org/10.1175/2011JHM1336.1

Hansen, J., Johnson, D., Lacis, A., Lebedeff, S., Lee, P., Rind, D., & Russell, G. (1981). Climate impact of increasing atmospheric carbon dioxide. *Science*, *213*(4511), 957–966. https://doi.org/10.1126/science.213.4511.957

Hearty, T. J. III, Lee, J. N., Wu, D. L., Cullather, R., Blaisdell, J. M., Susskind, J., & Nowicki, S. M. (2018). Intercomparison of Surface Temperatures from AIRS, MERRA, and MERRA-2 with NOAA and GC-Net Weather Stations at Summit, Greenland. *Journal of Applied Meteorology and Climatology*, *57*(5), 1231–1245.

Hingane, L. S., Kumar, K. R., & Murty, B. V. R. (1985). Long-term trends of surface air temperature in India. *Journal of Climatology*, *5*(5), 521–528. https://doi.org/10.1002/joc.3370050505

Hoffmann, P., Katzfey, J. J., McGregor, J. L., & Thatcher, M. (2016). Bias and variance correction of sea surface temperatures used for dynamical downscaling. *Journal of Geophysical Research: Atmospheres*, *121*, 12–877. https://doi.org/10.1002/2016JD025383

Houghton, J. T., Ding, Y. H., Griggs, D. J., Noguer, M., van der Linden, P. J., Dai, X., et al. (2001). *The scientific basis. Contribution of Working Group I to the Third Assessment Report of the Intergovernmental Panel on Climate Change*. Cambridge: Cambridge University Press.

Hu, Y., Dong, W., & He, Y. (2010). Impact of land surface forcings on mean and extreme temperature in eastern China. *Journal of Geophysical Research*, *115*, D19117. https://doi.org/10.1029/2009JD013368

IPCC (2001). The scientific basis. In J. T. Houghton, Y. Ding, D. J. Griggs, M. Noguer, P. J. Vander Linden, X. Dai, et al. (Eds.), *Contribution of Working Group I to the Third Assessment Report of the Intergovernmental Panel on Climate Change* (881 pp.). Cambridge: Cambridge University Press.

IPCC (2007). Climate change 2007: the physical science basis. In S. Solomon, D. Qin, M. Manning, Z. Chen, M. Marquis, K. B. Averyt, et al. (Eds.), *Contribution of Working Group I to the Fourth Assessment Report of the Intergovernmental Panel on Climate Change*. Cambridge: Cambridge University Press.

IPCC (2014). Climate Change 2014: Synthesis Report. In Core Writing Team, R. K. Pachauri, & L. A. Meyer (Eds.), *Contribution of Working Groups I, II and III to the Fifth Assessment Report of the Intergovernmental Panel on Climate Change* (151 pp.). Geneva, Switzerland: IPCC.

Jones, P. D., Wigley, T. M. L., & Kelly, P. M. (1982). Variations in surface air temperatures: Part 1. Northern Hemisphere, 1881–1980. *Monthly Weather Review*, *110*(2), 59–70.

Kleist, D. T., Parrish, D. F., Derber, J. C., Treadon, R., Errico, R. M., & Yang, R. (2009). Improving incremental balance in the GSI 3DVAR analysis system. *Monthly Weather Review*, *137*(3), 1046–1060. https://doi.org/10.1175/2008MWR2623.1

Kothawale, D. R., & Rupa Kumar, K. (2005). On the recent changes in surface temperature trends over India. *Geophysical Research Letters*, *32*, L18714. https://doi.org/10.1029/2005GL023528

Lai, Y. J., Li, C. F., Lin, P. H., Wey, T. H., & Chang, C. S. (2012). Comparison of MODIS land surface temperature and ground-based observed air temperature in complex topography. *International Journal of Remote Sensing*, *33*(24), 7685–7702.

Lavaysse, C., Vrac, M., Drobinski, P., Lengaigne, M., & Vischel, T. (2012). Statistical downscaling of the French Mediterranean climate: Assessment for present and projection in an anthropogenic scenario. *Natural Hazards and Earth System Science, Copernicus Publications on be-half of the European Geosciences Union, 2012*, *12*(3), 651–670. https://doi.org/10.5194/NHESS-12-651-2012.hal-00753343

Li, H., Sheffield, J., & Wood, E. F. (2010). Bias correction of monthly precipitation and temperature fields from Intergovernmental Panel on Climate Change AR4 models using equidistant quantile matching. *Journal of Geophysical Research*, *115*, D10101. https://doi.org/10.1029/2009JD012882

Liu, W., Chen, S., Jiang, H., Wang, C., & Li, D. (2017). Spatiotemporal analysis of MODIS land surface temperature with in situ meteorological observation and ERA-Interim Reanalysis: The option of model calibration. *IEEE J-STARS*, *10*(4), 1357–1371. https://doi.org/10.1109/JSTARS.2016.2645859

Maity, R., Suman, M., Laux, P., & Kunstmann, H. (2019). Bias correction of zero-inflated RCM precipitation fields: A copula-based scheme for both mean and extreme conditions. *Journal of Hydrometeorology*, *20*(4), 595–611. https://doi.org/10.1175/JHM-D-18-0126.1

Mao, G., Vogl, S., Laux, P., Wagner, S., & Kunstmann, H. (2015). Stochastic bias correction of dynamically downscaled precipitation fields for Germany through copula-based integration of gridded observation data. *Hydrology and Earth System Sciences*, *19*(4), 1787–1806. https://doi.org/10.5194/hess-19-1787-2015

Maraun, D., Shepherd, T. G., Widmann, M., Zappa, G., Walton, D., Gutiérrez, J. M., & Mearns, L. O. (2017). Towards process-informed bias correction of climate change simulations. *Nature Climate Change*, *7*(11), 764. https://doi.org/10.1038/NCLIMATE3418

McCarty, W., L. Coy, R. Gelaro, A. Huang, D. Merkova, E. B. Smith, et al., (2016). MERRA-2 input observations: Summary and initial assessment. Technical Report Series on Global Modeling and Data Assimilation, Vol. 46, NASA Tech. Rep. NASA/TM–2016–104606, 61 pp. [Available online at https://gmao.gsfc.nasa.gov/pubs/docs/McCarty885.pdf.]

Michelangeli, P. A., Vrac, M., & Loukos, H. (2009). Probabilistic downscaling approaches: Application to wind cumulative distribution functions. *Geophysical Research Letters*, *36*, L11708. https://doi.org/10.1029/2009GL038401

Molod, A., Takacs, L., Suarez, M., & Bacmeister, J. (2015). Development of the GEOS-5 atmospheric general circulation model: Evolution from MERRA to MERRA2. *Geoscientific Model Development*, *8*(5), 1339–1356. https://doi.org/10.5194/gmd-8-1339-2015

Rajeevan, M., Srivastava, A. K., & Kshirsagar, S. R. (2008). Development of a high resolution daily gridded temperature data set (1969–2005) for the Indian Region. In NCC Research Report 8. National Climate Centre India Meteorological Department.

Vigaud, N., Vrac, M., & Caballero, Y. (2013). Probabilistic downscaling of GCM scenarios over southern India. *International Journal of Climatology*, *33*(5), 1248–1263. https://doi.org/10.1002/joc.3509

Willmott, C. J. (1984). On the evaluation of model performance in physical geography. In *Spatial statistics and models* (pp. 443–460). Dordrecht: Springer.

Willmott, C. J. (1987). Models, climatic. In J. E. Oliver & R. W. Fairbridge (Eds.), *Encyclopedia of climatology* (pp. 584–590). New York: Van Nostrand Reinhold.

Willmott, C. J., & Matsuura, K. (2006). On the use of dimensioned measures of error to evaluate the performance of spatial interpolators. *International Journal of Geographical Information Science*, *20*(1), 89–102. https://doi.org/10.1080/13658810500286976